TET1 promotes growth of T-cell acute lymphoblastic leukemia and can be antagonized via PARP inhibition

Shiva Bamezai[1], Deniz Demir[1], Alex Jose Pulikkottil [1], Fabio Ciccarone[2], Elena Fischbein[1], Amit Sinha[3], Chiara Borga[4], Geertruy te Kronnie[4], Lüder-Hinrich Meyer[5], Fabian Mohr[1], Maria Götze[1], Paola Caiafa[6], Klaus-Michael Debatin[5], Konstanze Döhner[7], Hartmut Döhner[7], Irene Gonzalez Menendez[8], Leticia Quintanilla-Fend[8], Tobias Herold[9,10], Irmela Jeremias[10,11,12], Michaela Feuring-Buske[1.7], Christian Buske[1*] and Vijay P.S. Rawat[1*].

1. Institute of Experimental Cancer Research, University Hospital of Ulm, Ulm, Germany
2. Department of Biology, University of Rome "Tor Vergata", Rome, Rome, Italy
3. Basepair, New York, NY, USA
4. Department of Women's and Children's Health, University of Padova, Padova, Italy
5. Department of Pediatrics and Adolescent Medicine, Ulm University Medical Center, Ulm, Germany
6. Department of Cellular Biotechnologies and Hematology, Sapienza University of Rome, Rome, Italy
7. Department of Internal Medicine III, University Hospital of Ulm, Ulm, Germany
8. Institute of Pathology, University of Tübingen, 72076 Tübingen, Germany
9. Department of Medicine III, University Hospital, LMU Munich, Munich, Germany
10. Research Unit Apoptosis in Hematopoietic Stem Cells, Helmholtz Center Munich, German Center for Environmental Health (HMGU), Munich, Germany

11. Department of Pediatrics, Dr. von Hauner Childrens Hospital, Ludwig Maximilians University, Munich, Germany

12. German Consortium for Translational Cancer Research (DKTK), Partnering Site Munich, Munich, Germany

* Corresponding author(s) –

Vijay P. S. Rawat, Ph.D.

E-Mail: vijay.rawat@uni-ulm.de

Christian Buske, M.D.

E-Mail: christian.buske@uni-ulm.de

Abstract

T-cell acute lymphoblastic leukemia (T-ALL) is an aggressive hematological cancer characterized by skewed epigenetic patterns, raising the possibility of therapeutically targeting epigenetic factors in this disease. Here we report that among different cancer types, epigenetic factor *TET1* is highly expressed in T-ALL and is crucial for human T-ALL cell growth *in vivo*. *Tet1* knockout mice and knockdown in human T-cells did not perturb normal T-cell proliferation, indicating that *TET1* expression is dispensable for normal T-cell growth. The promotion of leukemic growth by TET1 was depending on its catalytic property to maintain global 5-hydroxymethylcytosine (5hmC) marks, thereby regulating cell cycle, DNA repair genes and T-ALL associated oncogenes. Furthermore, overexpression of the Tet1 catalytic domain was sufficient to augment global 5hmC levels and leukemic growth of T-ALL cells *in vivo*. We demonstrate that PARP enzymes, which are highly expressed in T-ALL patients, participate in establishing H3K4me3 marks at the TET1 promoter and that PARP1 interacts with the TET1 protein. Importantly, the growth related role of TET1 in T-ALL could be antagonized by the clinically approved PARP inhibitor Olaparib, which abrogated TET1 expression, induced loss of 5hmC marks and antagonized leukemic growth of T-ALL cells, opening a therapeutic avenue for this disease.

Introduction

Aberration in DNA methylation patterns are hallmarks of most human cancers and recent studies demonstrate that loci specific hypomethylation can transcriptionally activate oncogenes in various cancers [1-6]. Ten Eleven Translocation dioxygenase (TET1-3) enzymes, actively mediate DNA hypomethylation via oxidation of DNA 5mC marks to 5-hydroxymethylcytosine (5hmC), and consequently impact gene expression and chromosomal stability [7-12]. Several lines of evidence suggest that TET family members (TET1-3) and 5hmC marks safeguard DNA integrity and act as tumour suppressors [13-15]. *TET1* has been reported as lower expressed in colon tumours [16] and in B-cell malignancies, while global loss of 5hmC marks has been reported in multiple cancers [17]. Loss of *Tet1* and combined loss of *Tet1* and *Tet2* promotes B-cell malignancies [18-20]. *Tet1* knockout mice suffer loss of 5hmC marks at promoters and gene bodies of DNA repair genes [20]. Moreover, 5hmC marks are significantly enriched at damaged DNA sites [21], substantiating the significance of TET enzymes and 5hmC marks for tumour suppression.

Conversely, *TET* genes and in particular, *TET1*, also exhibit an oncogenic role in several malignancies [22-25], as shown for acute myeloid leukemia (AML)[20, 26]. Although *TET1* is translocated in rare cases in AML [27], the aberrant and high expression of the TET1 protein regulates the expression of critical oncogenic pathways in AML cells [26, 28]. These studies suggest that TET1 has dichotomous and context dependent roles in hematological malignancies. In the case of T-ALL, TET1 has been found mutated 1 in 264 T-ALL cases [29]. Nevertheless, the role of TET1 in T-ALL is poorly understood.

T-ALL is an aggressive hematological cancer originating from the malignant transformation of immature T-cell progenitors [30, 31]. Therapy outcome for T-ALL is significantly inferior compared to that for precursor B-ALL [32]. Relapse of the disease is the most common cause of treatment failure and is often linked to epigenetic mechanisms [33], pointing to the potential of therapies

targeting epigenetic factors for treating this malignancy. Recent studies in healthy human $CD4^+$ naïve T-cells indicate that TET1 negatively regulates Th1/Th2 differentiation by suppressing the expression of pro-differentiation genes such as *GATA3*, CD69 and IFNG *in vitro* growth promoting. In this study, we now demonstrate that in human T-ALL cells, high TET1 expression maintains global hydroxymethylome which positively regulates gene expression, safeguards genome integrity, and thereby promotes leukemic growth. Furthermore, our data indicate that the growth promoting activity of TET1 can be pharmacologically targeted via inhibition of PARPs, which act as TET1 upstream regulators, opening a potential treatment modality for T-ALL patients.

Materials and Methods

Patient samples and leukemic cell lines

Mononuclear cells isolated from diagnostic BM or PB samples from patients with T-ALL, B-ALL and AML, were analyzed. T-All and B-ALL samples were obtained from the University Hospital Ulm at diagnosis from pediatric patients (<18 yrs old) with de novo BCP-ALL after informed consent was given in accordance with the institution's ethical review board. For further information, see Supplementary information (SI).

Xenograft experiments (NSG)

All mice experiments were conducted according to the national animal welfare law (Tierschutzgesetz) and were approved by the Regierungspräsidium Tübingen, Germany. For assessing the impact of TET1 KD on T-ALL cell lines, NSG (NOD.Cg-PrkdcScid Il2rgtm1Wjl/SzJ) mice were injected intravenously, sacrificed 8 weeks hence and engraftment was confirmed by flow cytometry using anti-human CD45+ and CD3+ antibody.

For further information, see SI.

Olaparib treatment of cell lines and primary cells

For liquid culture assays, $1x10^5$ T-ALL cell lines were treated with Olaparib (5uM) or DMSO and growth kinetics were assayed over 6 days. For colony assays, 500 input cells were seeded into methylcellulose (H4330) containing Olaparib (5uM) or DMSO. The colonies were scored 14 days later.

Additional Materials and methods are described in Supplementary Methods

Results

TET1 is highly expressed in majority of T-ALL patients

Our initial analysis of *TET1* expression in published gene expression data sets of human cancer cell lines and leukemia patients revealed that *TET1* is highly expressed in T-ALL cell lines and highest in T-ALL patients among all leukemia types (Fig. S1A-B) [34, 35]. Our quantitative real time PCR (qRT-PCR) and gene expression microarray confirmed that *TET1* is several fold higher expressed in T-ALL patients and cell lines compared to other acute leukemia (Fig. 1A-B; Fig. S1C; Suppl. Table 1-2). Furthermore, our data and re-analysis of publically available cDNA microarray and RNA-seq data sets indicated that *TET1* is overexpressed in T-ALL patients compared to healthy bone marrow (BM) derived $CD34^+$ hematopoietic stem progenitors (HSPCs), BM derived $CD3^+$ T-cells and naïve T-cells (Fig. S1D-E) [29, 36]. Furthermore, western blots confirmed that TET1 protein is overexpressed in T-ALL cell lines compared to $CD3^+$ T-cells (Fig. 1C).

Adolescent and young adult T-ALL patients exhibited a trend towards higher *TET1* expression in comparison to elderly patients (Fig. S1F). Within the cohort of childhood cases, *TET1* was significantly higher expressed in the medium and high risk group compared to standard risk T-ALL (Fig. 1D). Expression levels of *TET1* were independent of the molecular cytogenetic subgroups or stages of maturation (Fig. S1G-H). However, in published RNA-seq data *TET1* was higher expressed in the subgroup harboring HOXA-rearrangements and in post-cortical stages of maturation (Fig. S1I-J) [29]. *TET1* expression was independent of the mutation status of recurrently mutated genes in T-ALL patients, such as NOTCH1 (Fig. S1K). Of note, the *TET1* paralogues - *TET2* and *TET3* – were not higher expressed in human T-ALL compared to other leukemia types or healthy BM (Fig. S1L-O).

TET1 is required for leukemic growth of human T-ALL cells but not critical for normal T-cell differentiation

Next, we sought to evaluate the functional relevance of high *TET1* expression in T-ALL cells. shRNA mediated depletion of *TET1* in T-ALL cell lines induced reduction of cell growth (70-80%) and colony numbers (50-95%) compared to scrambled control in liquid culture and colony forming unit (CFU) assays, respectively (Fig. S2A; Fig. 2A-B). NSG mice transplanted with TET1 depleted T-ALL cell lines showed a marked decrease in leukemic engraftment (Fig. 2C). Histopathological analysis revealed a sharp decrease in infiltration of human $CD3^+$ T-ALL cells in liver and lung (Fig. 2D). In T-ALL patient derived xenograft (PDX) cells, TET1 depletion caused a decrease in leukemic engraftment in BM and spleen, reflected in the reduced spleen sizes and spleen weight of xenografts (Fig. 2E-F).

To negate the possibility of an off-target effect of the shRNA, fist we transduced a TET1 expression lacking lymphoma cell line RAJI with shRNA against *TET1*. Second, we knocked out *TET1* by lentivirally overexpressing Cas9 and sgRNA targeting *TET1* (sgTET1) in T-ALL cell lines. The overexpression of shTET1A-B in RAJI did not impact proliferation or colony formation (Fig. 2A-B). However, as observed in our knockdown study, TET1 knockout in the bulk T-ALL cells induced a significantly reduction in CFU of T-ALL cell lines (Fig. S2B) and liquid culture proliferation (data not shown). The knockout of TET1 was evidenced by the reduction of TET1 protein in western blot (Fig. S2C), T7 endonuclease assay and sanger sequencing (data not shown).

To assess whether TET1 also has an important role in healthy T- cells, we knocked down TET1 in human T-cells and utilized *Tet1* knockout (ko) mice to analyze the effect on normal T-cell distribution [37]. In *Tet1* ko mice, no significant differences were observed in the absolute cell

numbers of the DN1-4 subpopulations or in $CD4^+$, $CD8^+$, $CD4^+$ $CD8^+$ (DP) subpopulations, albeit a trend towards a decrease in DN1, DN2 and particularly $CD4^+$ $CD8^+$ (DP) cells was observed (Fig. S2D-E). Notably in the spleen, BM and peripheral blood (PB) of young (8-12 weeks) ko and wt mice, no differences were observed in the distribution of $CD4^+$, $CD8^+$ and $CD4^+CD8^+$ T-cells, indicating that Tet1 is not essential for early T cell development in the thymus or for the formation of mature T-cells (Fig.2G) [37]. Furthermore, to test whether the absence of *Tet1* expression impairs expansion of T cells, we harvested splenic $CD3^+$ T-cells from wt and ko mice and subjected them to *in vitro* IL-2 stimulation. In the absence of *Tet1* expression, T-cells did not show any significant change in expansion *in vitro* (Fig. S2F). Moreover, we extended this analysis to human T-cells by knocking down *TET1* in $CD3^+$ T-cells enriched from PB. Similar to murine T-cells, TET1 depletion also did not exhibit any impact on IL-2 stimulated expansion of human T-cells (Fig. S2G).

Taken together our data suggests that high *TET1* expression is required to sustain leukemic growth of T-ALL cells but is not crucial for normal T-cell differentiation and growth.

The enzymatic domain of Tet1 is sufficient to rescue TET1 depleted cells and augment leukemic growth of human T-ALL

Next, we sought to examine whether the growth promoting function of TET1 in T-ALL cells is dependent on its enzymatic function. For this, we overexpressed only the catalytic domain of Tet1, (Tet1-CD) in the TET1 depleted T-ALL cell line JURKAT. The catalytic activity of Tet1 was sufficient to rescue TET1 depleted T-ALL cells *in vitro* and *in vivo* (Fig. 3A-C).

We previously performed gene expression analysis on primary T-ALL patient samples (n=5) pre and post-xenograft transplantation [38]: analysis of *TET1* expression in this dataset revealed a higher expression of *TET1* post-transplantation in 4 out of 5 xenografts compared to cells pre-

transplantation (Fig. S2H). Moreover, in a published microarray analysis of T-ALL cell lines transplanted into xenografts, a similar increase in *TET1* expression was observed (Fig. S2I), suggesting that high *TET1* expression is associated with leukemic growth *in vivo* [39]. Indeed, forced expression of Tet1-CD in T-ALL cell lines significantly augmented leukemic growth *in vitro* and *in vivo* (Fig. 3D-E). These data clearly suggest that the growth-promoting role of TET1 in T-ALL is at least partly dependent on its enzymatic activity.

TET1 depletion induces loss of 5hmC marks at promoters and gene bodies of genes involved in cell cycle, DNA repair and *NOTCH* pathway

Next we analyzed 5hmC levels in T-ALL cells via Intracellular fluorescence (IF) in our knockdown, rescue and overexpression experiments. IF-flow cytometry for 5hmC marks in TET1 depleted JURKAT cells, primary T-ALL patients and TET1 knockout bulk T-ALL cell lines revealed a significant decrease in global 5hmC levels (Fig. 4A-B and Fig. S3A-B) and increase in 5mC levels (Fig. S3C). Conversely, overexpression of Tet1-CD in TET1 depleted cells or wild type T-ALL cells induced a global increase in 5hmC levels (Fig. 4C-D).

Furthermore, we performed hydroxymethylated DNA immunoprecipitation (hMeDIP)-seq in TET1 depleted JURKAT cells. In hMeDIP-seq, TET1 depletion resulted in more than a 59% reduction of global 5hmC enrichment at the promoter (-5kbTSS), gene body (GB) and intergenic regions compared to scrambled control (referred to as TET1 dependent 5hmC or T1-5hmC regions from here) (Fig. 4E-F). In detail, a total of 2,404 and 6,115 5hmC enriched promoters and GB were observed in the scrambled arm, respectively, out of which more than 50% of the promoters and GB lost 5hmC marks upon TET1 depletion (Suppl. Table 3). On the contrary, in the absence of TET1, the majority of enhancers and superenhancers gained 5hmC marks, while only 206 enhancers and 75 superenhancers lost 5hmC marks (Suppl. Table 3). Collectively, these

data indicate that a large number of 5hmC enriched promoters are dependent on TET1 expression in T-ALL, particularly since *TET2* and *TET3* expression remained unchanged in *TET1* depleted and knockout bulk JURKAT and MOLT-4 cells (Fig. S3D-E).

Nearly 50% of T1-5hmC genes were known targets of TET1 in human embryonic stem cells [40] (Fig. 4F). 56% of T1-5hmC promoters and GB also harbored H3K4me3 marks on their promoters and less than 14% were associated with repressive H3K27me3 marks, reaffirming a functional role of TET1 in positive gene regulation (Fig. 4F-G; Suppl. Table 4). Notably, H3K4me3 associated T1-5hmC genes were enriched for cell cycle and DNA repair (Fig. 4H). Moreover, *RBPJ*, *NOTCH2* and *NOTCH3* - NOTCH signaling pathway genes, which play a critical role in the pathobiology of T-ALL, also lost 5hmC marks upon TET1 depletion. Of note, the majority (90%) of T1-5hmC promoters and gene bodies found in the JURKAT cell line were also enriched for 5hmC marks in healthy human naïve T-cells (Fig. S3F-G) [41].

TET1 and T1-5hmC marks are associated with gene expression of oncogenic and DNA repair pathways

To understand the relationship between T1-5hmC marks and gene expression, we reanalyzed the published microarray data of T-ALL patients (n=174) based on *TET1* expression [35]. We grouped patients into four quartiles based on TET1 expression levels and compared the gene expression pattern in the highest expressing group ($TET1^{high}$) versus the lowest expressing group ($TET1^{low}$): 1,659 genes were differentially expressed in $TET1^{high}$ vs $TET1^{low}$ patients of which 82% of the genes showed a positive association with high *TET1* expression (Fig. S4A-C). Genes positively associated with *TET1* expression in T-ALL were involved in regulation of cell cycle (dimerization partner, RB-like, E2F and multi-vulval class B (DREAM) complex targets), G2M checkpoint repair and breast cancer associated pathways (Fig. 5A, Fig. S4D-E; Suppl. Table 4).

314 genes that positively correlated with *TET1* expression in patients, lost 5hmC marks (promoter/GB) in the *TET1* depleted T-ALL cell line, JURKAT. Again, these genes were significantly enriched for cell cycle and DNA repair pathways (Fig. 5B; Suppl. Table 5). In RNA-seq analysis of *TET1* depleted JURKAT cells, 1,145 genes were differentially expressed, of which 70.8% were downregulated compared to the scrambled control (Fig. 5C; Suppl. Table 6). "*Hypoxia*" and "*mTORC1*" signaling pathways, which drive leukemic growth in T-ALL and *IL2-STAT5* signaling which is important for the TET1 driven oncogenic program in AML cells [28] were significantly downregulated upon Tet1 depletion (Fig. 5D) [42, 43]. (Suppl. Table 6). Notably, 89 genes associated with high *TET1* expression in patients also exhibited differential expression in our RNA-seq dataset (Suppl. Table 6). Amongst these were cell cycle, DNA repair genes (*RNF168, DTL, DCK, GINS3, AJUBA, CDK18, CDK19, RFC3 and TDG*) and oncogenes *NOTCH3*. Importantly, DNA repair genes (such as *BRCA1-2, RNF168, RAD51C, CDK18, CDK19, DTL, DCK*) and oncogenes (such as *NOTCH3*) that exhibited positive correlation with high *TET1* expression in T-ALL patients and lost 5hmC marks upon TET1 depletion, also exhibited deregulated expression in our RNA-seq and/or in qRTPCR data Fig. S4F). Moreover, DNA repair genes in TET1 knockout T-ALL cell lines and primary T-ALL patient cells showed a trend towards decreased expression (Fig. S4G-H). The decrease in expression was confirmed at the protein level in TET1 depleted JURKAT cells (Fig. S4I).

Our hMeDIP-seq and gene expression data in TET1 knockdown/knockout T-ALL cells, T-ALL patient microarray dataset and published TET1 ChIP-seq data, together strongly indicated that NOTCH3 is a downstream target of TET1 in T-ALL cells (Fig. S4F-H, Suppl. Table 3 and 6) [40]. Moreover, the depletion of NOTCH3 in T-ALL cell lines also induced a marked reduction in colony forming ability *in vitro* (Fig. S4J).

Depletion of TET1 impairs DNA repair in T-ALL cells

Since our data showed a link between expression of *TET1* and DNA repair genes in T-ALL, we analyzed whether TET1 depletion induces DNA damage in T-ALL cells. We observed an increase in total γH2AX protein levels and significantly increased numbers of γH2AX foci in TET1 depleted and bulk knockout T-ALL cells (Fig. 5E-F; Fig. S4K). Furthermore, neutral comet assays in cell lines and primary patient samples showed a significant increase in mean tail moment, indicating increased DNA damage induced by TET1 depletion (Fig. 5G-H). BrdU-Cell cycle analysis in TET1 depleted and bulk knockout T-ALL cells revealed a block in the G2/M phase compared to the scrambled arm (Fig. 5I; Fig. S4L). Exposure of T-ALL cell lines to DNA damage inducing γ-radiation triggered an increase in *TET1* expression by 50% (±11%, n=3) within 30 minutes post-exposure. *TET2* and *TET3* expression levels remained unchanged (Fig. 5J; Fig. S4M). Furthermore, depletion of TET1 rendered T-ALL cell lines sensitive to γ-radiation at ow dose of 0.5Gy and higher dose of 2Gy at a greater order than scrambled transduced cells (Fig. 5K). Taken together, these data strongly suggest that high TET1 expression protects T-ALL cells from DNA damage.

The PARP inhibitor Olaparib antagonizes TET1 induced T-ALL growth

We previously showed that the PARP enzyme activity (PARylation) positively regulates *TET1* expression via the epigenetic marks H3K4me3 [44]. Interestingly, several members of the PARP gene family are overexpressed in T-ALL patients compared to B-ALL patients and exhibit a trend towards higher expression compared to healthy T-cells (Fig. S5A). Furthermore, in JURKAT, the promoter of *TET1* displayed high enrichment for H3K4me3, H3Ac marks and lower enrichment levels for repressive H23K27me3 marks (Fig. S5B). Moreover, a CpG island in the TET1 promoter region was hypomethylated in the T-ALL cell lines and hypermethylated

in the low *TET1* expressing B-ALL cell lines (Fig. S5C). Based on these data we reasoned that high PARP expression in T-ALL could regulate TET1 expression via euchromatic epigenetic marks. Therefore, we blocked PARP enzymatic activity via treatment of T-ALL cell lines with Olaparib, an inhibitor of PARylation. Olaparib treatment lead to a significant reduction in *TET1* transcription and a concomitant decrease in H3K4me3 and H3Ac levels on the *TET1* promoter (Fig. 6A-B). Of note, *TET2*-3 expression was not affected (Fig. S5D-E). Olaparib treatment also resulted in reduced TET1 protein levels (Fig. 6C). Furthermore, co-immunoprecipitation (co-IP) assay showed that TET1 physically interacted with PARP1 in the T-ALL cell line JURKAT (Fig. 6D). In light of our observations, we reasoned that PARP mediated PARylation could also impact TET1 protein expression post-transcriptionally. To test this hypothesis, we transiently overexpressed Myc-tagged TET1 and Myc-tagged-Tet1-CD under the CMV promoter in HEK 293T cell and treated the cells with Olaparib for 72h. Olaparib treatment lead to the decrease of exogenous tagged protein levels compared to the DMSO control (Fig. 6E-F), suggesting that PARylation and PARP-1 interaction with TET1 impacts the protein stability of both the full length as well as Tet1-CD. These data indicate that TET1 is regulated transcriptionally and post-transcriptionally via PARylation, opening up a therapeutic opportunity to test whether the inhibition of PARylation via Olaparib could be used to target TET1 function in T-ALL.

Treatment with Olaparib induced marked reduction in colony formation of T-ALL cell lines accompanied by increased apoptosis of primary T-ALL primary patient samples compared to the DMSO control (Fig. 7A-B). JURKAT cells treated with Olaparib *in vit*ro for 48h and transplanted into NSG mice showed a significant reduction in BM engraftment (Fig. 7C). Histopathology analysis showed visible decrease in infiltration of human $CD3^+$ T-ALL cells in liver and lung of the drug treated arm (Fig. 7D). The treatment of PDX cells with Olaparib nearly abolished leukemic growth *in vivo* which was reflected in significantly reduced engraftment in

BM and spleen and reduced spleen sizes and weight (Fig. 7E-F). Furthermore, TET1 depleted T-ALL cells were more sensitive to Olaparib treatment and exhibited virtually no clonogenic potential in CFC assays (data not shown).

The block of PARylation activity via Olaparib induced a significant reduction in global 5hmC levels in T-ALL cell lines (Fig. 7G). Similar to shRNA mediated TET1 depletion, Olaparib treated JURKAT cells exhibited a trend towards a block in the G2M phase of the cell cycle and increased accumulation of γH2AX foci (Fig. 7H, Fig. S5F). Importantly, depletion of PARP1 via shRNA reduced *TET1* expression and markedly affected T-ALL cell line growth, indicating that *PARP* genes function upstream of TET1 in T-ALL cells (Fig. S5G-H). Lastly, we attempted to rescue the impact of Olaparib with overexpression of Tet1-CD in JURKAT cells. The ectopic overexpression of Tet1-CD marginally rescued the impact of Olaparib on T-ALL cell growth *in vitro* (Fig. S5I). Olaparib did not affect the exogenous expression of Tet1-CD (Fig. S5J). However, as shown before, Olaparib reduced the stability of the Tet1-CD protein contributing to the limited effect of Tet1-CD overexpression on the impact of Olaparib treatment (Fig. 6E-F).

Taken together, our data show that Olaparib is highly effective in counteracting the growth promoting effect of TET1 in human T-ALL.

Discussion

TET1 has dual roles in myeloid and lymphoid hematological malignancies [20, 26]. Our study showed that even within lymphoid leukemias, TET1 plays dichotomous roles as we demonstrated that TET1 exerts a growth-promoting role in T-ALL in contrast to B-cell malignancies in which TET1 acts as a tumor suppressor [20]: first we observed that among leukemias *TET1* is highly expressed in the majority of T-ALL patients. *TET1* was found higher expressed in patients compared to healthy thymic progenitors, adult naïve T-cells and BM derived T- cells, although we could not compare the expression levels in patients to primitive normal human double negative and double positive thymocytes, as these cells were not accessible. Secondly, leukemic growth of primary human T-ALL was dependent on high *TET1* expression, in contrast to normal T-cells as our characterization of young *Tet1* ko mice (8-12 weeks) and published data of older mice (24 weeks) indicated that Tet1 is not critical for *in vivo* T-cell development. Thirdly, the enhancement of the leukemic potential via overexpression of the Tet1 enzymatic domain and the increase in *TET1* expression in clonally expanded primary T-ALL cells *in vivo* indicated that high TET1 enzymatic activity is advantageous for the leukemic growth of T-ALL cells.

Mechanistically, TET1 achieves this growth promoting function in T-ALL by regulating 5hmC marks and thereby maintaining gene expression of factors required for growth and genomic integrity of T-ALL cells. TET1 depletion leads to loss of 5hmC marks (T1-5hmC) at cell cycle, DNA repair and gene expression associated genes, while the majority (70%) of differentially expressed genes upon TET1 depletion are downregulated, especially genes coding for factors required for cell cycle, DNA repair and oncogenic pathways. Furthermore, *TET1* expression in patients and also correlates with the cell cycle and DNA repair pathways. Thus, these data

indicate an active growth promoting role of TET1 in T-ALL, in contrast to healthy human T-cells, in which TET1 has been suggested to largely perform a repressive function [41].

Another known mechanism of cancer cells to maintain oncogenic growth and chemoresistance is to protect the cell from DNA damage [45, 46]. Indeed, in line with hMeDIP-seq and gene expression analysis, our data confirmed that TET1 protects the genomic integrity of T-ALL cells as depletion of TET1 resulted in DNA damage and enhanced sensitivity to IR exposure. Furthermore, induction of DNA damage via IR exposure prompted increase in *TET1* expression and an expression pattern reminiscent of the kinetics of γH2AX levels in radiation exposed cells [47, 48]. It is known that 5hmC marks also exhibit similar kinetics in response to IR, are significantly enriched at the sites of DNA damage and vital for ensuring genome integrity [21, 49, 50]. Therefore, the TET1 depletion induced loss of 5hmC marks in T-ALL cells could also render T-ALL cells more susceptible to DNA damage. Furthermore, we demonstrated that PARP1 induced *TET1* expression and interacts with the TET1 protein. Of note PARP1 itself has a known role in single strand DNA damage repair [15, 51]. Therefore, high TET1 expression and T1-5hmC marks could also promote growth of T-ALL cells by not only regulating expression of DNA repair genes but also by protecting the genome from damage by maintaining 5hmC marks at DNA lesions [52, 53].

Several studies indicate that *TET* genes have grossly unique functions in normal and malignant hematopoiesis [18-20, 37, 54-56]. Our data also suggests that the DNA repair function of TET1 is not compensated by other TET family members in T-ALL; for instance, *TET2-3* expression was not altered in our knockdown experiments, 5hmC levels remained low upon *TET1* depletion and exposure to radiation did not prompt changes in expression of *TET2-3*.

One of the major challenges is to translate these biological insights into new therapeutic strategies: in this context, PARP enzymes that are highly expressed in T-ALL patients and

regulate TET1 expression transcriptionally and post-transcriptionally, can be targeted using inhibitors [51, 57]. Inhibition of PARPs via Olaparib antagonizes the enzymatic activity of TET1, thereby abrogating leukemic growth of T-ALL cells *in vivo* opening a therapeutic avenue in this subtype of aggressive leukemias. The fact that Olaparib is clinically approved and T-ALL cells are sensitive to PARP inhibition should facilitate the initiation of clinical trials to test this therapeutic concept [58]. Interestingly, PARP inhibitors are highly effective in combating neuroblastoma and small lung cancer [59-63]. TET1 is highly expressed in both of these cancers (Fig. S1A) [34].

Based on our study we propose a model that high *TET1* expression sustains and promotes leukemic growth of transformed T-ALL cells via two proposed mechanisms (Fig. S6): high TET1 levels in T-ALL are transcriptionally and post-transcriptionally regulated by enzymatic activity of PARP family members. PARylated TET1 establishes 5hmC marks and positively regulates the expression of genes required for the growth and maintenance of genomic integrity of T-ALL cells (A). Furthermore, based on our own data and published studies we propose that the PARP1-TET1 complex and T1-5hmC marks also act as sensors at DNA lesions to promote DNA repair in T-ALL cells (B). Based on this, inhibition of PARylation will impair establishment of 5hmC marks, transcription of growth promoting genes and will induce an accumulation of DNA damage in T-ALL cells (A-B).

Author Contributions

V.P.S.R. designed the project. S.B., D.S., A.P.J., E.F. and F.C. performed experiments and S.B., G.K., C.Bo., M.F.B., C.B. and V.P.S.R. analyzed the data. A.S., S.B. and V.P.S.R. performed the RNA-seq, ChIP-seq data analysis and F.M. and T.H. performed the microarray analysis. L.Q.M. and I.G.M. performed histopathology. C.B., L.H.M., K.M.D, P.C., I.J., T.H., K.D. and H.D. contributed research material. S.B., C.Bo., G.T.K., L.H.M., T.H., V.P.S.R., and C.B. contributed to interpretation of patient data. S.B., C.B. and V.P.S.R. wrote the manuscript.

Disclosure of Conflicts of Interest

The authors declare no competing financial interests.

Acknowledgements

The authors would like to thank all members of the animal facility of the University of Ulm, Germany, for breeding and maintenance of the animals. The work was supported by a grant received by V.P.S.R. from the Ministry of Science, Research and the Art (MWK), Baden-Württemberg, Germany (Junior-professor Program, D.4268) and Baustein program 3.2, University of Ulm, Germany. F.C. is supported by a fellowship from the Italian Foundation for Cancer Research (AIRC). T.H. is supported by a Physician Scientists Grant from the Helmholtz Zentrum München. C.B. and M.F.-B. were funded by grants from the DFG (SFB 1074 project A4 to CB and A6 to M.F.-B.). Furthermore, we thank Medhanie A. Mulaw for his advice, participation in fruitful discussions and helping in analysis of RNA-seq data. We would also like to thank Dr. Dinesh Adhikary and Prof. Joseph Mautner for their support with T-cell assays.

406 **Supplementary Information**

407 Supplementary information includes, methods, supplementary figures (Fig.S1-6), figure legends
408 and supplementary tables (Table S1-6).

409

References

1. Bedford MT, van Helden PD. Hypomethylation of DNA in pathological conditions of the human prostate. *Cancer Res* 1987 Oct 15; **47**(20)**:** 5274-5276.

2. Lin CH, Hsieh SY, Sheen IS, Lee WC, Chen TC, Shyu WC*, et al.* Genome-wide hypomethylation in hepatocellular carcinogenesis. *Cancer Res* 2001 May 15; **61**(10)**:** 4238-4243.

3. Kim YI, Giuliano A, Hatch KD, Schneider A, Nour MA, Dallal GE*, et al.* Global DNA hypomethylation increases progressively in cervical dysplasia and carcinoma. *Cancer* 1994 Aug 1; **74**(3)**:** 893-899.

4. Perez RF, Tejedor JR, Bayon GF, Fernandez AF, Fraga MF. Distinct chromatin signatures of DNA hypomethylation in aging and cancer. *Aging Cell* 2018 Mar 5.

5. Zelic R, Fiano V, Grasso C, Zugna D, Pettersson A, Gillio-Tos A*, et al.* Global DNA hypomethylation in prostate cancer development and progression: a systematic review. *Prostate Cancer Prostatic Dis* 2015 Mar; **18**(1)**:** 1-12.

6. Wahlfors J, Hiltunen H, Heinonen K, Hamalainen E, Alhonen L, Janne J. Genomic hypomethylation in human chronic lymphocytic leukemia. *Blood* 1992 Oct 15; **80**(8)**:** 2074-2080.

7. Tahiliani M, Koh KP, Shen Y, Pastor WA, Bandukwala H, Brudno Y*, et al.* Conversion of 5-methylcytosine to 5-hydroxymethylcytosine in mammalian DNA by MLL partner TET1. *Science* 2009 May 15; **324**(5929)**:** 930-935.

8. Ito S, D'Alessio AC, Taranova OV, Hong K, Sowers LC, Zhang Y. Role of Tet proteins in 5mC to 5hmC conversion, ES-cell self-renewal and inner cell mass specification. *Nature* 2010 Aug 26; **466**(7310)**:** 1129-1133.

9. Ito S, Shen L, Dai Q, Wu SC, Collins LB, Swenberg JA*, et al.* Tet proteins can convert 5-methylcytosine to 5-formylcytosine and 5-carboxylcytosine. *Science* 2011 Sep 2; **333**(6047)**:** 1300-1303.

10. Wu H, D'Alessio AC, Ito S, Wang Z, Cui K, Zhao K*, et al.* Genome-wide analysis of 5-hydroxymethylcytosine distribution reveals its dual function in transcriptional regulation in mouse embryonic stem cells. *Genes Dev* 2011 Apr 1; **25**(7)**:** 679-684.

11. Xu Y, Wu F, Tan L, Kong L, Xiong L, Deng J*, et al.* Genome-wide regulation of 5hmC, 5mC, and gene expression by Tet1 hydroxylase in mouse embryonic stem cells. *Mol Cell* 2011 May 20; **42**(4)**:** 451-464.

12. Yang J, Guo R, Wang H, Ye X, Zhou Z, Dan J*, et al.* Tet Enzymes Regulate Telomere Maintenance and Chromosomal Stability of Mouse ESCs. *Cell Rep* 2016 May 24; **15**(8)**:** 1809-1821.

13. Moran-Crusio K, Reavie L, Shih A, Abdel-Wahab O, Ndiaye-Lobry D, Lobry C*, et al.* Tet2 loss leads to increased hematopoietic stem cell self-renewal and myeloid transformation. *Cancer Cell* 2011 Jul 12; **20**(1)**:** 11-24.

14. An J, Gonzalez-Avalos E, Chawla A, Jeong M, Lopez-Moyado IF, Li W*, et al.* Acute loss of TET function results in aggressive myeloid cancer in mice. *Nat Commun* 2015 Nov 26; **6:** 10071.

15. Weber AR, Krawczyk C, Robertson AB, Kusnierczyk A, Vagbo CB, Schuermann D*, et al.* Biochemical reconstitution of TET1-TDG-BER-dependent active DNA demethylation reveals a highly coordinated mechanism. *Nat Commun* 2016 Mar 2; **7:** 10806.

16. Neri F, Dettori D, Incarnato D, Krepelova A, Rapelli S, Maldotti M*, et al.* TET1 is a tumour suppressor that inhibits colon cancer growth by derepressing inhibitors of the WNT pathway. *Oncogene* 2015 Aug 6; **34**(32)**:** 4168-4176.

17. Rasmussen KD, Helin K. Role of TET enzymes in DNA methylation, development, and cancer. *Genes Dev* 2016 Apr 1; **30**(7)**:** 733-750.

18. Li Z, Cai X, Cai CL, Wang J, Zhang W, Petersen BE*, et al.* Deletion of Tet2 in mice leads to dysregulated hematopoietic stem cells and subsequent development of myeloid malignancies. *Blood* 2011 Oct 27; **118**(17)**:** 4509-4518.

19. Zhao Z, Chen L, Dawlaty MM, Pan F, Weeks O, Zhou Y*, et al.* Combined Loss of Tet1 and Tet2 Promotes B Cell, but Not Myeloid Malignancies, in Mice. *Cell Rep* 2015 Nov 24; **13**(8)**:** 1692-1704.

20. Cimmino L, Dawlaty MM, Ndiaye-Lobry D, Yap YS, Bakogianni S, Yu Y*, et al.* TET1 is a tumor suppressor of hematopoietic malignancy. *Nat Immunol* 2015 Jun; **16**(6)**:** 653-662.

21. Kafer GR, Li X, Horii T, Suetake I, Tajima S, Hatada I*, et al.* 5-Hydroxymethylcytosine Marks Sites of DNA Damage and Promotes Genome Stability. *Cell Rep* 2016 Feb 16; **14**(6)**:** 1283-1292.

22. Wang J, Li F, Ma Z, Yu M, Guo Q, Huang J*, et al.* High Expression of TET1 Predicts Poor Survival in Cytogenetically Normal Acute Myeloid Leukemia From Two Cohorts. *EBioMedicine* 2018 Feb; **28:** 90-96.

23. Hahn MA, Qiu R, Wu X, Li AX, Zhang H, Wang J*, et al.* Dynamics of 5-hydroxymethylcytosine and chromatin marks in Mammalian neurogenesis. *Cell Rep* 2013 Feb 21; **3**(2)**:** 291-300.

24. Wu MZ, Chen SF, Nieh S, Benner C, Ger LP, Jan CI*, et al.* Hypoxia Drives Breast Tumor Malignancy through a TET-TNFalpha-p38-MAPK Signaling Axis. *Cancer Res* 2015 Sep 15; **75**(18)**:** 3912-3924.

25. Yokoyama S, Higashi M, Tsutsumida H, Wakimoto J, Hamada T, Wiest E*, et al.* TET1-mediated DNA hypomethylation regulates the expression of MUC4 in lung cancer. *Genes Cancer* 2017 Mar; **8**(3-4)**:** 517-527.

26. Huang H, Jiang X, Li Z, Li Y, Song CX, He C*, et al.* TET1 plays an essential oncogenic role in MLL-rearranged leukemia. *Proc Natl Acad Sci U S A* 2013 Jul 16; **110**(29)**:** 11994-11999.

27. Lorsbach RB, Moore J, Mathew S, Raimondi SC, Mukatira ST, Downing JR. TET1, a member of a novel protein family, is fused to MLL in acute myeloid leukemia containing the t(10;11)(q22;q23). *Leukemia* 2003 Mar; **17**(3)**:** 637-641.

28. Jiang X, Hu C, Ferchen K, Nie J, Cui X, Chen CH*, et al.* Targeted inhibition of STAT/TET1 axis as a therapeutic strategy for acute myeloid leukemia. *Nat Commun* 2017 Dec 13; **8**(1)**:** 2099.

29. Liu Y, Easton J, Shao Y, Maciaszek J, Wang Z, Wilkinson MR*, et al.* The genomic landscape of pediatric and young adult T-lineage acute lymphoblastic leukemia. *Nat Genet* 2017 Aug; **49**(8)**:** 1211-1218.

30. Peirs S, Van der Meulen J, Van de Walle I, Taghon T, Speleman F, Poppe B*, et al.* Epigenetics in T-cell acute lymphoblastic leukemia. *Immunol Rev* 2015 Jan; **263**(1)**:** 50-67.

31. Girardi T, Vicente C, Cools J, De Keersmaecker K. The genetics and molecular biology of T-ALL. *Blood* 2017 Mar 2; **129**(9)**:** 1113-1123.

32. Vitale A, Guarini A, Ariola C, Mancini M, Mecucci C, Cuneo A*, et al.* Adult T-cell acute lymphoblastic leukemia: biologic profile at presentation and correlation with response to induction treatment in patients enrolled in the GIMEMA LAL 0496 protocol. *Blood* 2006 Jan 15; **107**(2)**:** 473-479.

33. Knoechel B, Roderick JE, Williamson KE, Zhu J, Lohr JG, Cotton MJ*, et al.* An epigenetic mechanism of resistance to targeted therapy in T cell acute lymphoblastic leukemia. *Nat Genet* 2014 Apr; **46**(4)**:** 364-370.

34. Barretina J, Caponigro G, Stransky N, Venkatesan K, Margolin AA, Kim S*, et al.* The Cancer Cell Line Encyclopedia enables predictive modelling of anticancer drug sensitivity. *Nature* 2012 Mar 28; **483**(7391)**:** 603-607.

35. Haferlach T, Kohlmann A, Wieczorek L, Basso G, Kronnie GT, Bene MC*, et al.* Clinical utility of microarray-based gene expression profiling in the diagnosis and subclassification of leukemia: report from the International Microarray Innovations in Leukemia Study Group. *J Clin Oncol* 2010 May 20; **28**(15)**:** 2529-2537.

36. Poole CJ, Lodh A, Choi JH, van Riggelen J. MYC deregulates TET1 and TET2 expression to control global DNA (hydroxy)methylation and gene expression to maintain a neoplastic phenotype in T-ALL. *Epigenetics Chromatin* 2019 Jul 2; **12**(1)**:** 41.

37. Dawlaty MM, Ganz K, Powell BE, Hu YC, Markoulaki S, Cheng AW*, et al.* Tet1 is dispensable for maintaining pluripotency and its loss is compatible with embryonic and postnatal development. *Cell Stem Cell* 2011 Aug 5; **9**(2)**:** 166-175.

38. Meyer LH, Eckhoff SM, Queudeville M, Kraus JM, Giordan M, Stursberg J*, et al.* Early relapse in ALL is identified by time to leukemia in NOD/SCID mice and is characterized by a gene signature involving survival pathways. *Cancer Cell* 2011 Feb 15; **19**(2)**:** 206-217.

39. Hollingshead MG, Stockwin LH, Alcoser SY, Newton DL, Orsburn BC, Bonomi CA*, et al.* Gene expression profiling of 49 human tumor xenografts from in vitro culture through multiple in vivo passages--strategies for data mining in support of therapeutic studies. *BMC Genomics* 2014 May 22; **15:** 393.

40. Verma N, Pan H, Dore LC, Shukla A, Li QV, Pelham-Webb B*, et al.* TET proteins safeguard bivalent promoters from de novo methylation in human embryonic stem cells. *Nat Genet* 2018 Jan; **50**(1)**:** 83-95.

41. Nestor CE, Lentini A, Hagg Nilsson C, Gawel DR, Gustafsson M, Mattson L*, et al.* 5-Hydroxymethylcytosine Remodeling Precedes Lineage Specification during Differentiation of Human CD4(+) T Cells. *Cell Rep* 2016 Jul 12; **16**(2)**:** 559-570.

42. Giambra V, Jenkins CE, Lam SH, Hoofd C, Belmonte M, Wang X*, et al.* Leukemia stem cells in T-ALL require active Hif1alpha and Wnt signaling. *Blood* 2015 Jun 18; **125**(25)**:** 3917-3927.

43. Evangelisti C, Ricci F, Tazzari P, Tabellini G, Battistelli M, Falcieri E*, et al.* Targeted inhibition of mTORC1 and mTORC2 by active-site mTOR inhibitors has cytotoxic effects in T-cell acute lymphoblastic leukemia. *Leukemia* 2011 May; **25**(5)**:** 781-791.

44. Ciccarone F, Valentini E, Bacalini MG, Zampieri M, Calabrese R, Guastafierro T*, et al.* Poly(ADP-ribosyl)ation is involved in the epigenetic control of TET1 gene transcription. *Oncotarget* 2014 Nov 15; **5**(21)**:** 10356-10367.

45. Turgeon MO, Perry NJS, Poulogiannis G. DNA Damage, Repair, and Cancer Metabolism. *Front Oncol* 2018; **8:** 15.

46. Torgovnick A, Schumacher B. DNA repair mechanisms in cancer development and therapy. *Front Genet* 2015; **6:** 157.

47. Redon CE, Dickey JS, Bonner WM, Sedelnikova OA. gamma-H2AX as a biomarker of DNA damage induced by ionizing radiation in human peripheral blood lymphocytes and artificial skin. *Adv Space Res* 2009; **43**(8)**:** 1171-1178.

48. Banath JP, Macphail SH, Olive PL. Radiation sensitivity, H2AX phosphorylation, and kinetics of repair of DNA strand breaks in irradiated cervical cancer cell lines. *Cancer Res* 2004 Oct 1; **64**(19)**:** 7144-7149.

49. Jiang D, Wei S, Chen F, Zhang Y, Li J. TET3-mediated DNA oxidation promotes ATR-dependent DNA damage response. *EMBO Rep* 2017 May; **18**(5)**:** 781-796.

50. Brennan CW, Verhaak RG, McKenna A, Campos B, Noushmehr H, Salama SR*, et al.* The somatic genomic landscape of glioblastoma. *Cell* 2013 Oct 10; **155**(2)**:** 462-477.

51. Ciccarone F, Valentini E, Zampieri M, Caiafa P. 5mC-hydroxylase activity is influenced by the PARylation of TET1 enzyme. *Oncotarget* 2015 Sep 15; **6**(27)**:** 24333-24347.

52. Coulter JB, Lopez-Bertoni H, Kuhns KJ, Lee RS, Laterra J, Bressler JP. TET1 deficiency attenuates the DNA damage response and promotes resistance to DNA damaging agents. *Epigenetics* 2017; **12**(10)**:** 854-864.

53. Zhong J, Li X, Cai W, Wang Y, Dong S, Yang J*, et al.* TET1 modulates H4K16 acetylation by controlling auto-acetylation of hMOF to affect gene regulation and DNA repair function. *Nucleic Acids Res* 2017 Jan 25; **45**(2)**:** 672-684.

54. Tsagaratou A, Gonzalez-Avalos E, Rautio S, Scott-Browne JP, Togher S, Pastor WA*, et al.* TET proteins regulate the lineage specification and TCR-mediated expansion of iNKT cells. *Nat Immunol* 2017 Jan; **18**(1)**:** 45-53.

55. Tsagaratou A, Lio CJ, Yue X, Rao A. TET Methylcytosine Oxidases in T Cell and B Cell Development and Function. *Front Immunol* 2017; **8:** 220.

56. Yue X, Trifari S, Aijo T, Tsagaratou A, Pastor WA, Zepeda-Martinez JA*, et al.* Control of Foxp3 stability through modulation of TET activity. *J Exp Med* 2016 Mar 7; **213**(3)**:** 377-397.

57. Roper SJ, Chrysanthou S, Senner CE, Sienerth A, Gnan S, Murray A*, et al.* ADP-ribosyltransferases Parp1 and Parp7 safeguard pluripotency of ES cells. *Nucleic Acids Res* 2014 Aug; **42**(14)**:** 8914-8927.

58. Parvin S, Ramirez-Labrada A, Aumann S, Lu X, Weich N, Santiago G*, et al.* LMO2 Confers Synthetic Lethality to PARP Inhibition in DLBCL. *Cancer Cell* 2019 Sep 16; **36**(3)**:** 237-249 e236.

59. Nile DL, Rae C, Hyndman IJ, Gaze MN, Mairs RJ. An evaluation in vitro of PARP-1 inhibitors, rucaparib and olaparib, as radiosensitisers for the treatment of neuroblastoma. *BMC Cancer* 2016 Aug 11; **16:** 621.

60. Sanmartin E, Munoz L, Piqueras M, Sirerol JA, Berlanga P, Canete A*, et al.* Deletion of 11q in Neuroblastomas Drives Sensitivity to PARP Inhibition. *Clin Cancer Res* 2017 Nov 15; **23**(22)**:** 6875-6887.

61. Jiang Y, Dai H, Li Y, Yin J, Guo S, Lin SY*, et al.* PARP inhibitors synergize with gemcitabine by potentiating DNA damage in non-small-cell lung cancer. *Int J Cancer* 2019 Mar 1; **144**(5)**:** 1092-1103.

62. Pietanza MC, Waqar SN, Krug LM, Dowlati A, Hann CL, Chiappori A*, et al.* Randomized, Double-Blind, Phase II Study of Temozolomide in Combination With Either Veliparib or Placebo in Patients With Relapsed-Sensitive or Refractory Small-Cell Lung Cancer. *J Clin Oncol* 2018 Aug 10; **36**(23)**:** 2386-2394.

63. Colicchia V, Petroni M, Guarguaglini G, Sardina F, Sahun-Roncero M, Carbonari M*, et al.* PARP inhibitors enhance replication stress and cause mitotic catastrophe in MYCN-dependent neuroblastoma. *Oncogene* 2017 Aug 17; **36**(33)**:** 4682-4691.

Figures Legends:

Fig. 1 *TET1* is highly expressed in T-ALL patients

(A) *TET1* mRNA expression values in human leukemia patients and healthy cells, determined by TaqMan qRT-PCR. Dots represent expression levels corresponding to independent biological replicates indicated as 'n'. Each box plot shows mean and range of expression. Fold values were obtained through normalization to expression of the housekeeping gene *TBP*. Statistical differences were calculated using one way-ANOVA **(B-D)** *TET1* expression assessed via cDNA microarray of **(B)** human leukemia patients from the Munich-Berlin data set: GSE66006 and GSE78132; statistical differences were calculated using one way-ANOVA **(C)** Western blot for TET1 protein in T-ALL cell lines compared to PB derived CD3+ T-cells. β-Actin was used as an endogenous control. **(D)** *TET1* expression in standard versus medium and high risk T-ALL patients, obtained using cDNA microarray (Munich-Berlin gene expression data set GSE66006 and GSE78132) *p<0.05; **p<0.001; ***p<0.0001

Fig. 2 TET1 is required for leukemic growth for human T-ALL

(A) Total cell number at day 6 in liquid culture expansion assay of T-ALL cell lines transduced with scrambled or shRNA. Bars represent mean cell number and error bars indicate standard error of mean (sem.); 'n' represents number of independent experiments performed for each cell line. Statistical differences were calculated using Kruskal–Wallis test **(B)** Colony assay of *TET1* depleted T-ALL cells versus scrambled control with 500 cells initially plated at day 0; Colonies were scored on day 14. Bars represent mean number of colonies and error bars indicate sem.; 'n' represents number of independent experiments. Statistical differences were calculated using Kruskal–Wallis test **(C)** Percentage of engrafted $CD45^+$ T-ALL cells in the BM of sacrificed NSG mice transplanted with scrambled control (Scr) or shRNA transduced T-ALL cell lines.

683 Each dot indicates percentage of $CD45^+$ cells in the BM of a single NSG mouse. Horizontal lines
684 indicate mean; statistical differences were calculated using two tailed t-test. **(D)**
685 Immunohistochemical staining of liver and lung tissue sections of NSG mice, verifying presence
686 of $CD3^+$ human T-ALL cells in sacrificed mice 8 weeks post-transplantation **(E)** Percentage of
687 human $CD45^+$ T-ALL cells in the BM and spleen of NSG mice transplanted with two separate
688 patient derived xenograft (PDX) samples, PDX#1-2, after transduction with scrambled control or
689 *TET-1* shRNA. Each dot indicates percentage of $CD45^+$ cells in a single NSG mouse BM.
690 Horizontal lines indicate mean **(F)** Spleen weight (in milligrams) of NSG mice transplanted with
691 scrambled control or shRNA transduced PDX cells sacrificed 8 weeks post-transplantation **(G)**
692 Percentage distribution of murine T-cell subpopulations in BM, spleen and peripheral blood of
693 aged matched *Tet1* wt and ko mice, analyzed by FACS. Bars indicate mean percentage and error
694 bars indicate stdev. 'n' represents biological replicates. Significant differences were calculated
695 using Mann Whitney test**.** *p<0.05; **p<0.001; ***p<0.0001
696
697 **Fig. 3 The enzymatic activity of TET1 is required for sustenance of T-ALL cells**
698 **(A-B)** JURKAT cells double-transduced with shTET1-B + Tet1-catalytic domain (CD) versus
699 shTET1-B + empty vector control (pCDH) **(A)** Total cell number at day 6 in liquid culture
700 expansion assay **(B)** Total number of colonies in the primary CFU assay per 500 input cells; bars
701 represent mean values, error bars indicate stdev; 'n' represents independent experiments,
702 significant differences were calculated using Mann Whitney test. **(C)** Percentage of $CD45^+$ T-
703 ALL cells in the BM, spleen and liver of NSG mice transplanted with FACS sorted shTET1-B +
704 Tet1-CD versus shTET1-B + pCDH transduced JURKAT cells. Each dot indicates percentage of
705 $CD45^+$ cells in a single NSG mouse. Horizontal bars represent average engraftment. Statistical
706 differences were calculated using t-test. **(D)** Total number of colonies in the CFU assay per 500

input cells in Tet1-CD or pCDH transduced JURKAT and MOLT-4 cell lines. Bars represent mean values; error bars indicate stdev; individual experiments are indicated as 'n'. Statistical differences were calculated using Mann Whitney test. **(E)** Percentage of $CD45^+$ T-ALL cells in the BM of NSG mice transplanted with pCDH and Tet1-CD transduced JURKAT cells. Each dot indicates percentage of $CD45^+$ cells in a single NSG mouse bone marrow. Horizontal bars represent average engraftment. Statistical differences were calculated using t-test.

Fig. 4 TET1 regulates 5hmC marks in T-ALL cells

(A) IF-flow cytometry of 5hmC in T-ALL cell line JURKAT. Bars represent mean values; error bars indicate standard deviation; independent experiments are indicated as 'n'. Statistical differences were calculated using one-way ANOVA **(B)** IF-confocal microscopy analysis of 5hmC in primary T-ALL patient cells. The plot represents the combined results of three independent experiments. The box plot represents the intensity of 5hmC marks in single cells. Horizontal bars indicate median intensity and vertical lines represent range of intensity. White line show 10μm. Statistical differences were calculated using Mann-Whitney test. **(C)** Total 5hmC content of shTET1-B + Tet1-CD versus shTET1-B + pCDH transduced JURKAT cells, as observed via IF-flow cytometry. Bars represent mean values; error bars indicate standard deviation; individual experiments are indicated as 'n'. Statistical differences were calculated using two tailed t-test. **(D)** IF-confocal microscopy analysis of JURKAT cells transduced with empty vector or Tet1-CD. IF-confocal microscopy analysis of 5hmC in primary T-ALL patient cells. The plot represents the combined results of three independent experiments. The box plot represents the intensity of 5hmC marks in single cells. Horizontal bars indicate median intensity and vertical lines represent range of intensity. White line show 10μm. Statistical differences were calculated using Mann-Whitney test. **(E)** hMeDIP-seq- percentage of losses and gains across

genomic regions in *TET1* depleted JURKAT cells versus scrambled control. **(F)** Heatmap shows centered 5hmC peaks, histone marks (activating marks H3K4me3 and repressive marks H3K27me3) and TET1 occupancy in the region of ±5kb TSS. In heatmaps (in green), the upper panel represents loci enriched with 5hmC marks in the scrambled arm but reduced or absent in the shRNA arm, while the lower panel shows regions enriched in the shRNA arm but reduced or absent in the scrambled arm. Blue heatmaps represent corresponding loci enriched with H3K4me3 and H3K27me3 marks in JURKAT cells, and TET1 occupancy (ChIP-seq) [40] in human ESC **(G)** Overlap of *TET1* dependent 5hmC promoters and gene bodies (T1-5hmC) with H3K4me3 and H3K27me3 enriched promoters in JURKAT cells **(H)** Top five Enrichr, Reactome 2016 pathways associated with T1-5hmC-H3K4me3 and T1-5hmC-H3K27me3 genes; p-value<0.05, FDR<0.05.

Fig. 5 High *TET1* expression protects T-ALL cells from DNA damage, accompanied by expression of cell cycle and DNA repair pathways

(A) Heatmap representing the expression of cell cycle and dimerization partner, RB-like, E2F and multi-vulval class B (DREAM) complex genes in high *TET1* expressing T-ALL patients (n=44) versus low *TET1* expressing patients (n=44) (Table S4A). **(B)** Reactome pathway analysis of T1-5hmC genes in JURKAT cells which correlated with *TET1* expression in T-ALL patients (FDR<0.05, p<0.05). **(C)** Heatmap showing selected differentially expressed genes in RNA-seq of TET1 depleted JURKAT cells (n=2, FDR<0.05, p<0.05) **(D)** GSEA analysis of RNA-seq of TET1 depleted JURKAT cells showing pathways downregulated after TET1 depletion. **(E)** Western blot of total phosphorylated H2AX (Ser139) levels in TET1 depleted T-ALL cell line JURKAT. H2A.X represents the endogenous control. **(F)** Representative IF image and summary of the percentage of cells harboring >5 phosphorylated H2AX (Ser139) foci in

scrambled vs shRNA transduced JURKAT cells. The graph represents the combined results of three independent experiments. Bars represent mean values and error bars represent stdev; White line represents distance of 10μm. Statistical differences were calculated using one-way ANOVA **(G)** Neutral comet assay in TET1 depleted JURKAT cells. The plot represents the combined results of three independent experiments. Horizontal lines represent the median and vertical lines represent range. Statistical differences were calculated using Mann-Whitney test. The representative figure shows comet tails highlighted by white arrows. **(H)** Neutral comet assay in TET1 depleted primary T-ALL patient samples. The plot represents the combined results of three independent experiments. Horizontal lines represent the median and vertical lines represent range. Statistical differences were calculated using Mann-Whitney test. **(I)** Cell cycle analysis of TET1 depleted JURKAT cells versus scrambled control 48h post-transduction using BrdU staining. Bars represent mean values and error bars represent stdev; 'n' represents number of independent experiments. Statistical differences were calculated using Kruskal-Wallis test **(J)** qRT-PCR gene expression analysis of *TET 1-3* in 2Gy γ-radiation exposed T-ALL cell lines, 30 mins post-exposure. Bars represent mean values and error bars represent stdev. 'n' represents number of independent experiments. Statistical differences were calculated using Kruskal-Wallis test **(K)** Viable cell number of *TET1* depleted vs scrambled control JURKAT cell line, 24h and 96h post-exposure to 0.5 and 2Gy γ-radiation analyzed by trypan blue exclusion. Dotted line depicts cell number at day 0 ($1x10^5$). Bars represent mean values and error bars represent stdev. 'n' represents number of independent experiments. Statistical differences were calculated using Kruskal-Wallis test. *$p<0.05$; **$p<0.001$; ***$p<0.0001$; ns. – not significant.

Fig. 6 Enzymatic activity of PARPs regulates *TET1* mRNA expression and protein stability in T-ALL cells

(A) *TET1* mRNA expression in T-ALL cell lines, quantified via qRT-PCR, 72h post-treatment with the PARylation inhibitor Olaparib versus DMSO control. Bars represent mean values, error bars represent stdev and 'n' represents independent experiments. Statistical differences were calculated using Mann-Whitney test **(B)** ChIP-qRT PCR of histone marks on the promoter of *TET1* 72h post Olaparib treatment vs. DMSO control in JURKAT cells (position from transcription start site (TSS): A (-200 to-100), B (-100 to +1) and C (+1 to +200). Bars represent mean values, error bars represent stdev and 'n' represents independent experiments. Statistical differences were calculated using Mann-Whitney test **(C)** TET1 protein levels in DMSO versus Olaparib treated JURKAT cells, 72h post-treatment assayed by Western blot and summarized via densitometry analysis. Bars represent mean values, error bars represent stdev and 'n' represent independent experiments. Statistical differences were calculated using paired t-test **(D)** Co-immunoprecipitation of endogenous PARP-1 with TET1 in JURKAT cells **(E-F)** TET1 protein levels in Olaparib or DMSO treated and transiently transfected HEK 293T cells expressing **(E)** Myc tagged full length TET1 construct and **(F)** Myc tagged Tet1-CD, 72h post-treatment, assayed by western blot using antibody against Myc tag. *p<0.05; **p<0.001; ***p<0.0001

Fig. 7 Olaparib treatment antagonizes TET1 expression and abrogates T-ALL cell growth *in vitro* and *in vivo*

(A) Total number of colonies in primary CFU assay per 500 input cells of Olaparib treated T-ALL cell lines vs DMSO control. Bars represent mean values, error bars represent stdev and 'n' represent independent experiments. Statistical differences were calculated using a two tailed t-test. **(B)** Annexin-V and 7-AAD staining of primary T-ALL patient cells, 72h post-treatment with Olaparib or DMSO. Bars represent mean values, error bars represent stdev and 'n' represents biological replicates. Statistical differences were calculated using Mann-Whitney test.

(C) Percentage of $CD45^+$ T-ALL cells in the BM of NSG mice transplanted with JURKAT cells treated *in vitro* with Olaparib or DMSO for 72h. Each dot indicates percentage of $CD45^+$ cells in a single NSG mouse. Horizontal bars represent average engraftment. Statistical differences were calculated using t-test. **(D)** Immunohistochemical staining of liver and lung tissue sections of NSG mice injected with Olaparib or DMSO treated JURKAT cells for quantifying $CD3^+$ human T-ALL cells (400X and 630X magnification). **(E)** Percentage of $CD45^+$ T-ALL PDX cells in the BM and spleen of sacrificed NSG mice transplanted with DMSO or Olaparib treated PDX sample, 8 weeks' post- transplantation. Each dot indicates percentage of $CD45^+$ cells in a single NSG mouse BM. Horizontal bars represent average engraftment. Statistical differences were calculated using t-test. **(F)** Spleen weight (in milligrams) of NSG mice transplanted with DMSO or Olaparib treated PDX cells, sacrificed 8 weeks' post- transplantation. Each dot indicates the spleen weight of a single mouse. Horizontal bars represent average spleen weight. Statistical differences were calculated using t-test. **(G)** Analysis of total 5hmC content in Olaparib vs DMSO treated JURKAT and CCRF-CEM cells, using DNA dot blot assay using anti-5hmC monoclonal antibody. **(H)** Cell cycle analysis of Olaparib treated JURKAT cells versus DMSO control 72h post-transduction using BrdU staining. Bars represent mean values, error bars represent stdev and 'n' represent independent experiments. Statistical differences were calculated using Mann-Whitney test. *$p<0.05$; **$p<0.001$; ***$p<0.0001$

Fig. 1

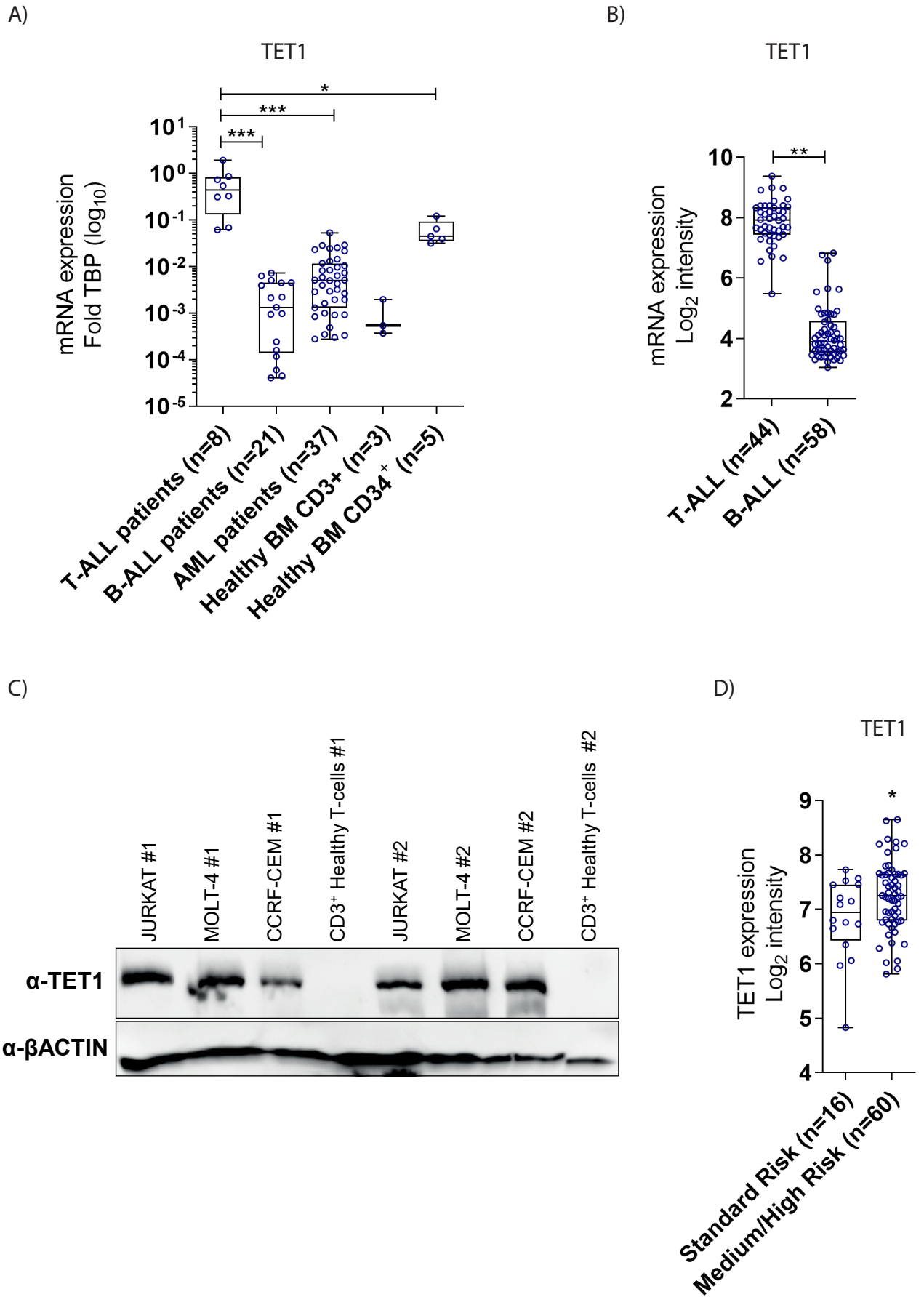
A)
TET1
mRNA expression
Fold TBP (log10)
*
***
***
T-ALL patients (n=8)
B-ALL patients (n=21)
AML patients (n=37)
Healthy BM CD3+ (n=3)
Healthy BM CD34+ (n=5)
B)
TET1
mRNA expression
Log2 intensity
**
T-ALL (n=44)
B-ALL (n=58)
C)
JURKAT #1
MOLT-4 #1
CCRF-CEM #1
CD3+ Healthy T-cells #1
JURKAT #2
MOLT-4 #2
CCRF-CEM #2
CD3+ Healthy T-cells #2
α-TET1
α-βACTIN
D)
TET1
TET1 expression
Log2 intensity
*
Standard Risk (n=16)
Medium/High Risk (n=60)

Fig. 2

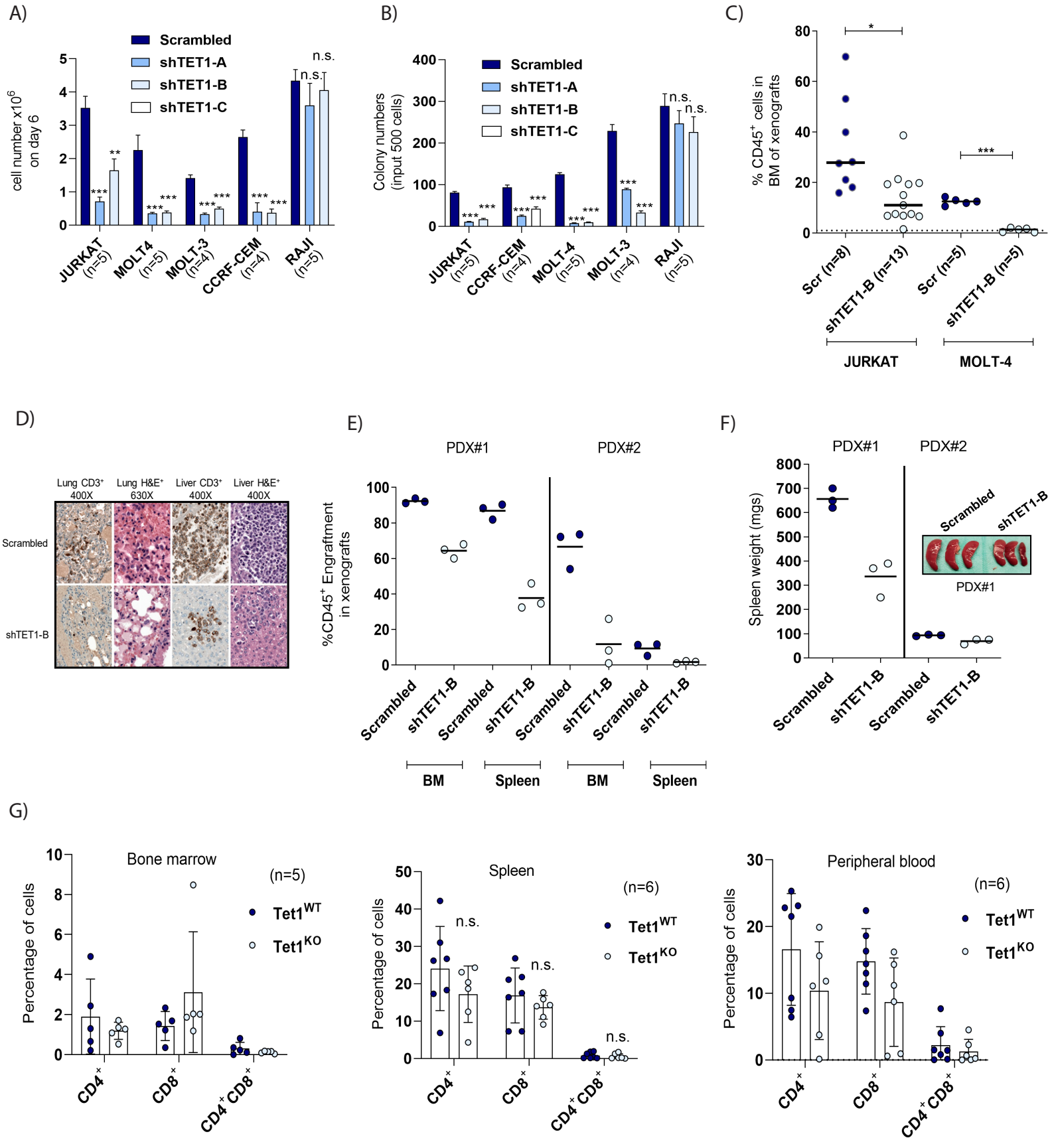
A)
Scrambled
shTET1-A
shTET1-B
shTET1-C
cell number x10^6 on day 6
JURKAT (n=5)
MOLT4 (n=5)
MOLT-3 (n=4)
CCRF-CEM (n=4)
RAJI (n=5)
n.s.
B)
Colony numbers (input 500 cells)
C)
% CD45+ cells in BM of xenografts
Scr (n=8)
shTET1-B (n=13)
Scr (n=5)
shTET1-B (n=5)
JURKAT
MOLT-4
D)
Lung CD3+ 400X
Lung H&E+ 630X
Liver CD3+ 400X
Liver H&E+ 400X
Scrambled
shTET1-B
E)
PDX#1
PDX#2
%CD45+ Engraftment in xenografts
BM
Spleen
F)
Spleen weight (mgs)
G)
Bone marrow
(n=5)
Tet1WT
Tet1KO
Percentage of cells
CD4+
CD8+
CD4+CD8+
Spleen
(n=6)
Peripheral blood

Fig. 3

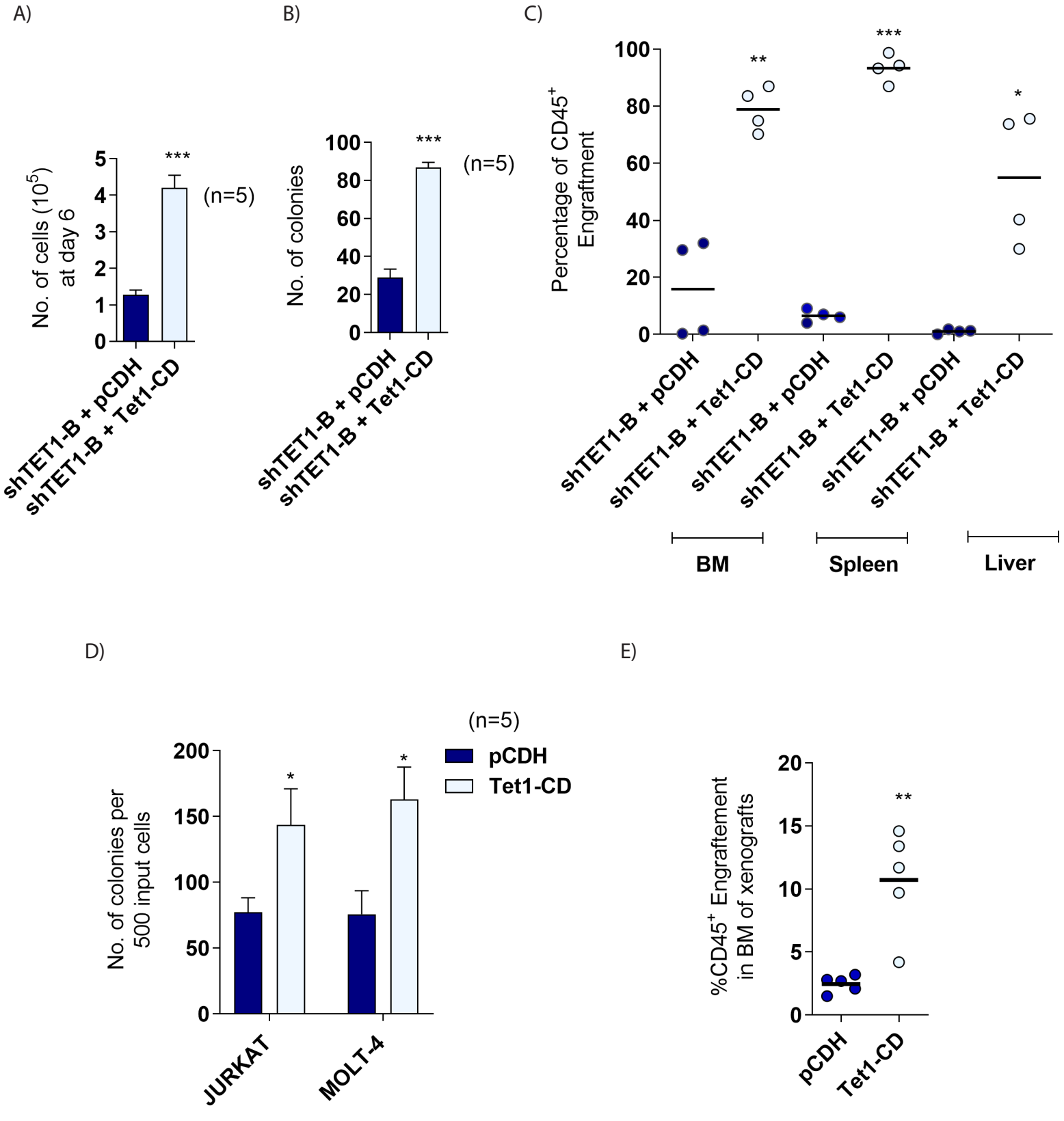
A)
No. of cells (10^5) at day 6
***
(n=5)
shTET1-B + pCDH
shTET1-B + Tet1-CD
B)
No. of colonies
***
(n=5)
shTET1-B + pCDH
shTET1-B + Tet1-CD
C)
Percentage of CD45+ Engraftment
**
***
*
shTET1-B + pCDH
shTET1-B + Tet1-CD
BM
Spleen
Liver
D)
No. of colonies per 500 input cells
(n=5)
pCDH
Tet1-CD
*
*
JURKAT
MOLT-4
E)
%CD45+ Engraftement in BM of xenografts
**
pCDH
Tet1-CD

Fig. 4

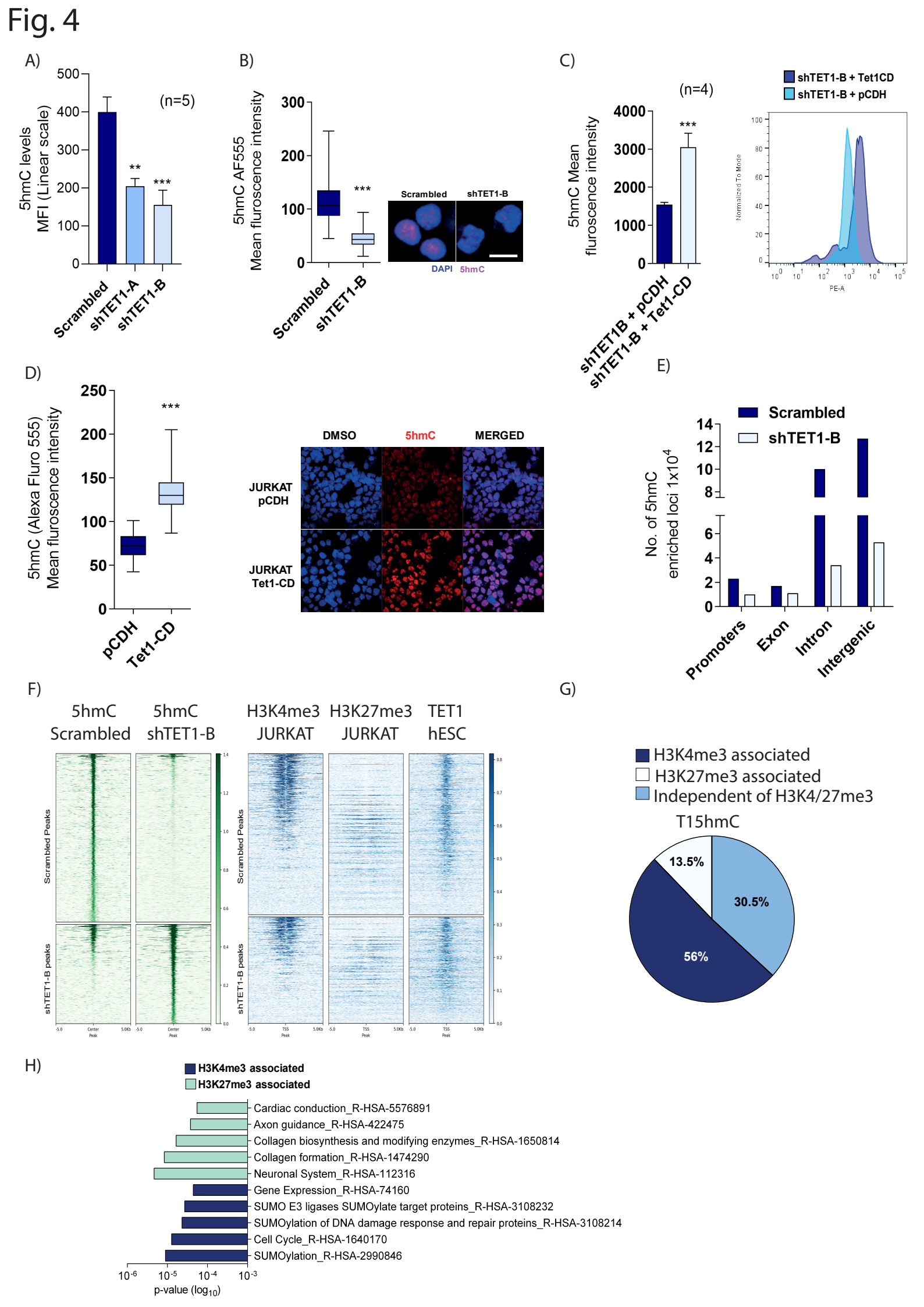
A)
5hmC levels
MFI (Linear scale)
(n=5)
**
***
Scrambled
shTET1-A
shTET1-B
B)
5hmC AF555
Mean fluroscence intensity
***
Scrambled
shTET1-B
Scrambled
shTET1-B
DAPI
5hmC
C)
(n=4)
5hmC Mean
fluroscence intensity
***
shTET1B + pCDH
shTET1-B + Tet1-CD
shTET1-B + Tet1CD
shTET1-B + pCDH
Normalized To Mode
PE-A
D)
5hmC (Alexa Fluro 555)
Mean fluroscence intensity
***
pCDH
Tet1-CD
DMSO
5hmC
MERGED
JURKAT
pCDH
JURKAT
Tet1-CD
E)
Scrambled
shTET1-B
No. of 5hmC
enriched loci 1x10^4
Promoters
Exon
Intron
Intergenic
F)
5hmC
Scrambled
5hmC
shTET1-B
H3K4me3
JURKAT
H3K27me3
JURKAT
TET1
hESC
Scrambled Peaks
shTET1-B peaks
Center
Peak
TSS
Peak
G)
H3K4me3 associated
H3K27me3 associated
Independent of H3K4/27me3
T15hmC
13.5%
30.5%
56%
H)
H3K4me3 associated
H3K27me3 associated
Cardiac conduction_R-HSA-5576891
Axon guidance_R-HSA-422475
Collagen biosynthesis and modifying enzymes_R-HSA-1650814
Collagen formation_R-HSA-1474290
Neuronal System_R-HSA-112316
Gene Expression_R-HSA-74160
SUMO E3 ligases SUMOylate target proteins_R-HSA-3108232
SUMOylation of DNA damage response and repair proteins_R-HSA-3108214
Cell Cycle_R-HSA-1640170
SUMOylation_R-HSA-2990846
p-value (log10)

Fig. 5

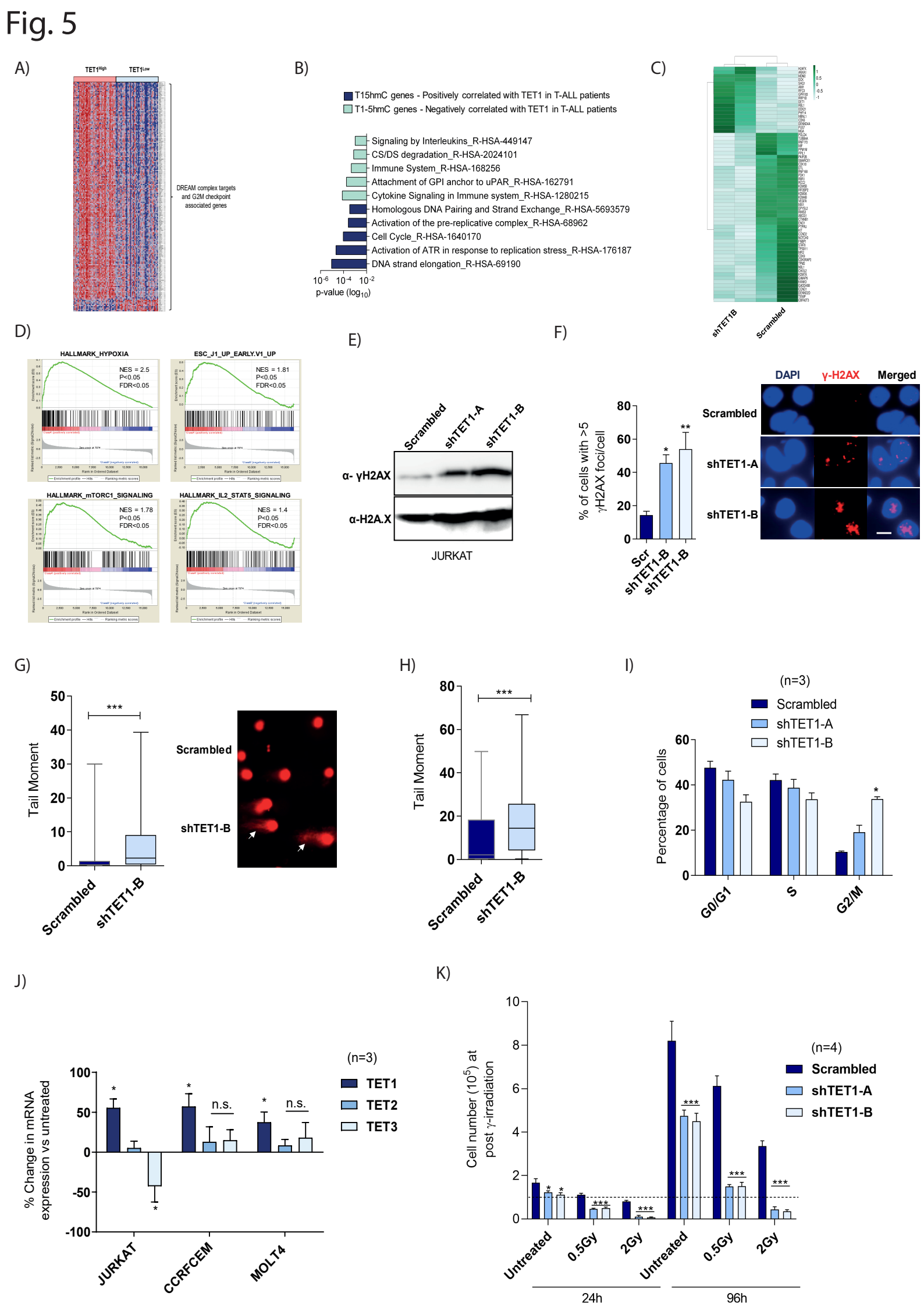
A)
TET1High
TET1Low
DREAM complex targets and G2M checkpoint associated genes
B)
T15hmC genes - Positively correlated with TET1 in T-ALL patients
T1-5hmC genes - Negatively correlated with TET1 in T-ALL patients
Signaling by Interleukins_R-HSA-449147
CS/DS degradation_R-HSA-2024101
Immune System_R-HSA-168256
Attachment of GPI anchor to uPAR_R-HSA-162791
Cytokine Signaling in Immune system_R-HSA-1280215
Homologous DNA Pairing and Strand Exchange_R-HSA-5693579
Activation of the pre-replicative complex_R-HSA-68962
Cell Cycle_R-HSA-1640170
Activation of ATR in response to replication stress_R-HSA-176187
DNA strand elongation_R-HSA-69190
p-value (log10)
C)
shTET1B
Scrambled
D)
HALLMARK_HYPOXIA
NES = 2.5
P<0.05
FDR<0.05
ESC_J1_UP_EARLY.V1_UP
NES = 1.81
P<0.05
FDR<0.05
HALLMARK_mTORC1_SIGNALING
NES = 1.78
P<0.05
FDR<0.05
HALLMARK_IL2_STAT5_SIGNALING
NES = 1.4
P<0.05
FDR<0.05
E)
Scrambled
shTET1-A
shTET1-B
α- γH2AX
α-H2A.X
JURKAT
F)
% of cells with >5 γH2AX foci/cell
Scr
shTET1-B
shTET1-B
DAPI
γ-H2AX
Merged
Scrambled
shTET1-A
shTET1-B
G)
Tail Moment
***
Scrambled
shTET1-B
H)
Tail Moment
***
Scrambled
shTET1-B
I)
(n=3)
Scrambled
shTET1-A
shTET1-B
Percentage of cells
G0/G1
S
G2/M
J)
% Change in mRNA expression vs untreated
(n=3)
TET1
TET2
TET3
n.s.
n.s.
JURKAT
CCRFCEM
MOLT4
K)
Cell number (10^5) at post γ-irradiation
(n=4)
Scrambled
shTET1-A
shTET1-B
Untreated
0.5Gy
2Gy
Untreated
0.5Gy
2Gy
24h
96h

Fig. 6

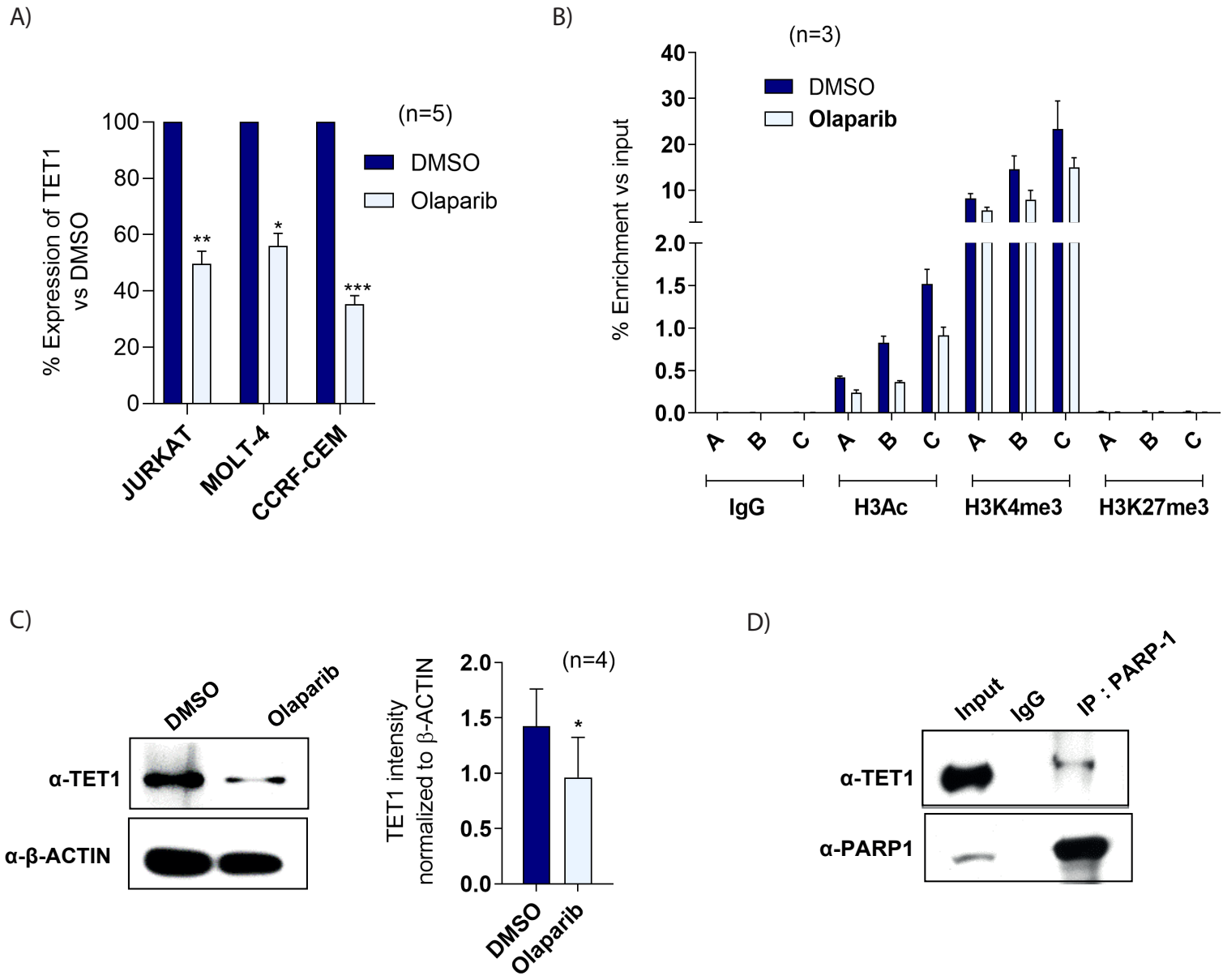
A)
% Expression of TET1 vs DMSO
(n=5)
DMSO
Olaparib
JURKAT
MOLT-4
CCRF-CEM
B)
(n=3)
DMSO
Olaparib
% Enrichment vs input
IgG
H3Ac
H3K4me3
H3K27me3
C)
DMSO
Olaparib
α-TET1
α-β-ACTIN
TET1 intensity normalized to β-ACTIN
(n=4)
D)
Input
IgG
IP : PARP-1
α-TET1
α-PARP1
E)
Olaparib 5uM
DMSO
α-Myc tag (TET1 WT)
α-LAMIN B
F)
DMSO
Olaparib 5uM
α-Myc tag (Tet1-CD)
α- LAMIN B

Fig. 7

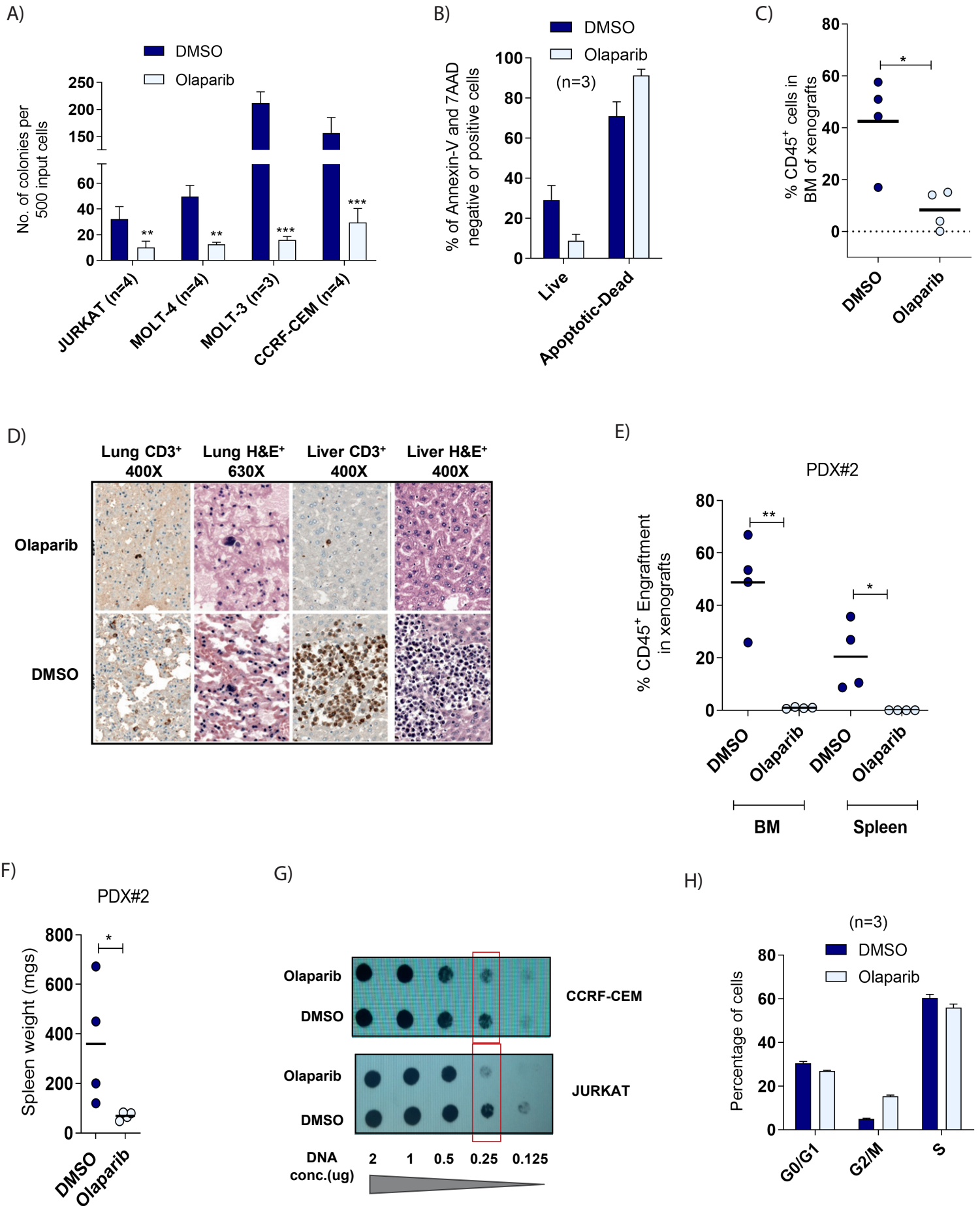
A)
DMSO
Olaparib
No. of colonies per 500 input cells
JURKAT (n=4)
MOLT-4 (n=4)
MOLT-3 (n=3)
CCRF-CEM (n=4)
B)
DMSO
Olaparib
(n=3)
% of Annexin-V and 7AAD negative or positive cells
Live
Apoptotic-Dead
C)
% CD45+ cells in BM of xenografts
DMSO
Olaparib
D)
Lung CD3+ 400X
Lung H&E+ 630X
Liver CD3+ 400X
Liver H&E+ 400X
Olaparib
DMSO
E)
PDX#2
% CD45+ Engraftment in xenografts
DMSO
Olaparib
DMSO
Olaparib
BM
Spleen
F)
PDX#2
Spleen weight (mgs)
DMSO
Olaparib
G)
Olaparib
DMSO
CCRF-CEM
Olaparib
DMSO
JURKAT
DNA conc.(ug)
2
1
0.5
0.25
0.125
H)
(n=3)
DMSO
Olaparib
Percentage of cells
G0/G1
G2/M
S